J. Fluid Mech. (1998), *vol.* 365, *pp.* 369–381. Printed in the United Kingdom

© 1998 Cambridge University Press

Stability of straining flow with surface cooling and temperature-dependent viscosity

By JONATHAN J. WYLIE AND JOHN R. LISTER

Institute of Theoretical Geophysics, Department of Applied Mathematics and Theoretical Physics, Silver Street, Cambridge CB3 9EW, UK

(Received 7 March 1997)

The stability of uniform straining flow in a semi-infinite body of viscous fluid subjected to surface cooling is examined. The viscosity of the fluid is assumed to be a prescribed function of temperature. If the viscosity variations caused by the cooling are sufficiently large the straining flow is linearly unstable to a mode in which the rate of extension of the viscous thermal boundary layer becomes localized. The parameters of the problem are the viscosity contrast in the fluid and a dimensionless measure of the rate of strain relative to the rate of cooling. The conditions under which instability occurs are determined and the physical mechanisms responsible are examined. The results are applied to discuss the formation of some surface features in lava flows.

1. Introduction

Many processes involve fluids which experience dramatic changes in viscosity when cooled. Examples include lava flows, convective processes in the mantle, various stages during the manufacture of glass and many other industrial processes. However, despite the obvious importance and prevalence of temperature-dependent flows there have been surprisingly few studies of them. In a number of applications fluids with a temperature-dependent viscosity are subjected to a straining flow and surface cooling.

The fluid adjacent to the base of a spreading viscous gravity current must satisfy the 'no-slip' condition, which gives rise to shear within the current. However, the surface area of the gravity current increases as it spreads, and thus the current, and in particular the surface, also experiences a strain. Thus the interior of the flow is a complicated mixture of shearing and straining. If the gravity current intrudes into a fluid of much lower viscosity (e.g. air or water) the surface shear stress is low (Huppert 1982; Lister 1992) and hence the flow in the vicinity of the surface is well approximated by a pure straining flow. We note that thermally induced variations in viscosity are often confined to the vicinity of the free surface where the cooling is greatest.

In viscous gravity currents that do not experience large viscosity contrasts, observations show that the surface of the current is remarkably smooth and uniform (Huppert 1982; Lister 1992). In contrast, when viscosity contrasts are large, uneven surface features are observed. One of the most spectacular instances of this can be seen in the uneven surface extension and folding observed in lava flows (e.g. Tepley & Moore 1974). While there is solidified material on the surface of lava flows, it forms a heavily fractured broken crust with cracks that penetrate into the incandescent molten interior (Crisp & Baloga 1990). This observation was used by Stasiuk, Jaupart

& Sparks (1993) to argue that the solid crust has negligible strength, which seems reasonable in extension or flexure, and to model the flow with a temperature-dependent Newtonian viscosity. In the problem considered here we make a similar assumption in order to isolate the interaction between extension and variable viscosity. We note, however, that a solidified crust can give rise to other phenomena, such as bridging of channelized flows.

There is a wide variation in the surface morphology of lava flows (Fink & Griffiths 1990; Hulme 1974; Keszthelyi & Denlinger 1996). In examples relevant here the lava fronts observed in the later stages of Hawaiian pahoehoe lava flows are characterized by the irregular development of small-scale lobes known as 'pahoehoe toes'. The fronts of submarine basaltic flows form uneven bulbous surface structures known as pillows. In each case, the bulk lava front is advancing slowly, constrained by a cooled surface layer. The toes and the pillows are formed when hot lava in the interior of the flow breaks through a weak point in the surface layer resulting in a relatively rapid advance and inflation of that part of the front. During the very early stages of the inflation the surface of the outbreak remains relatively smooth. However, as the front spreads, the surface cools, the rate of expansion slows and surface features on the scale of a few millimetres to centimetres are formed. The outbreak then continues to expand more slowly until it is cooled to the temperature of the remainder of the surface. The process then begins again with localization of the surface strain to form a new toe or pillow. On a larger scale the localized breakout that forms the pillow or toe can be regarded as the nonlinear evolution of an instability of the bulk lava front as the front is slowly stretched by the advance of the flow. It is the evolution of such cooled straining surfaces that we propose to model.

Some qualitative comparison may also be drawn with flow of the Earth's mantle which is known to exhibit large viscosity contrasts between the hot interior and the cold surface layer or lithosphere. Both at mid-ocean ridges and when a hot ascending plume nears the surface, the surface layer is significantly strained and the strain localizes along the mid-ocean ridge axis or along rift zones above the plume.

In this study we consider the fundamental problem of a fluid with temperature-dependent viscosity being subjected to a straining flow and surface cooling by radiation. The stability analysis uses a form of frozen-field approximation for the modal dependence normal to the interface, but accounts fully for modal stretching parallel to the interface. We show that, given sufficient variation in viscosity, such cooled straining flows can become unstable and give rise to surface perturbations. We determine the conditions under which instability occurs and discuss the physical nature of the instability. We note that in subaerial lava flows the cooling is typically dominated by radiation, whereas submarine flows lose most of their heat by convection into the water (Fink & Griffiths 1990). While we have chosen here to focus on radiative cooling, we expect similar results to apply when the cooling is due to convection.

2. Formulation

Consider a semi-infinite region of fluid under the influence of a straining flow driven at infinity with strain rate Γ (figure 1). The straining flow is oriented such that the direction of extension is parallel to the unperturbed free surface with the stagnation point of the flow positioned on the unperturbed free surface. We choose coordinates x and y such that the origin is at the stagnation point with the x-direction aligned with the unperturbed free surface.

The fluid is assumed to be of constant density ρ and thermal diffusivity κ, and

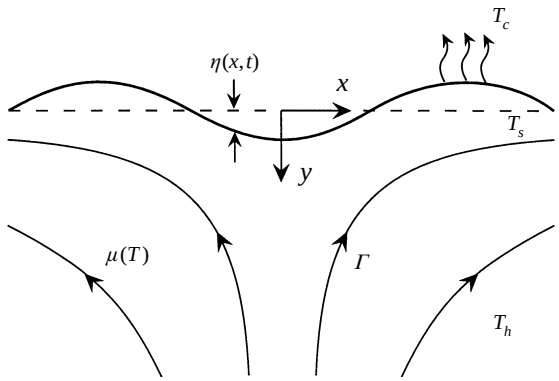

FIGURE 1. Definition sketch. A semi-infinite fluid with temperature-dependent viscosity $\mu(T)$ is driven by a straining flow Γ imposed at infinity. The temperature of the fluid at depth is T_h and the free surface is cooled to a temperature T_s by radiation to an overlying environment maintained at temperature T_c. The interface is perturbed to $y = \eta(x,t)$.

the viscosity is assumed to be a function only of the temperature. Far from the free surface the fluid is maintained at a temperature $T = T_h$. We suppose that the variation of the fluid viscosity with temperature is given by $\mu(T)$ and take the viscosity far from the free surface $\mu_h = \mu(T_h)$ as the reference value in dimensional scalings. The surface is radiatively cooled by an overlying environment which is maintained at a temperature T_c.

We neglect the effects of mechanical inertia, gravity, surface tension and viscous heating, which is usually valid in the applications envisaged to flows of lava or glass. For example, to estimate these effects in lava flows we take parameter values $\rho \sim 3000\,\mathrm{kg\,m^{-3}}$, $\kappa \sim 10^{-6}\,\mathrm{m^2\,s^{-1}}$, $\mu_h \sim 10^2 - 10^7\,\mathrm{Pa\,s}$, $\Gamma \sim 10^{-2}$–$1\,\mathrm{s^{-1}}$, $T_h - T_c \sim 10^3\,\mathrm{K}$, surface-tension coefficient $\gamma \sim 10^{-1}\,\mathrm{kg\,s^{-2}}$ and specific heat capacity $c_p \sim 10^3\,\mathrm{J\,kg^{-1}\,K^{-1}}$. We use the thermal boundary-layer thickness $(\kappa/\Gamma)^{1/2}$ as the relevant lengthscale. On this lengthscale inertial terms in the momentum equation are negligible compared to viscous terms because of large Prandtl number

$$Pr = \frac{\mu_h}{\rho\kappa} \sim 3 \times 10^4 \gg 1. \tag{2.1}$$

Gravitationally induced pressure differences which flatten surface perturbations are negligible compared to viscous stresses since

$$\frac{\bar{\mu}\Gamma}{\rho g(\kappa/\Gamma)^{1/2}} \sim 3 \times 10^3 \gg 1, \tag{2.2}$$

where we take $\bar{\mu} = 10^4\,\mathrm{Pa\,s}$ as a typical surface viscosity and g is the acceleration due to gravity. Stresses due to surface tension are negligible compared with viscous stresses since

$$\frac{\bar{\mu}\Gamma}{\gamma(\Gamma/\kappa)^{1/2}} \sim 10^3 \gg 1. \tag{2.3}$$

Finally, heat generated by viscous heating is negligible compared with that associated with external temperature differences since

$$\frac{\mu_h\Gamma}{\rho c_p(T_h - T_c)} \sim 3 \times 10^{-8} \ll 1. \tag{2.4}$$

We denote the velocity by (u, v), the pressure by p and the free-surface displacement

by η. We define dimensionless variables by

$$\hat{T} = \frac{T - T_c}{T_h - T_c}, \quad \hat{\mu} = \frac{\mu(T)}{\mu_h}, \quad \hat{t} = \frac{\Gamma}{2}t, \tag{2.5 a–c}$$

$$(\hat{x}, \hat{y}, \hat{\eta}) = \left(\frac{\Gamma}{2\kappa}\right)^{1/2}(x, y, \eta), \quad \hat{p} = \frac{2}{\mu_h \Gamma}p \quad \text{and} \quad (\hat{u}, \hat{v}) = \left(\frac{2}{\Gamma\kappa}\right)^{1/2}(u, v). \tag{2.5 d–f}$$

As a result of the assumptions (2.1)–(2.4) and non-dimensionalization (2.5), the equations of motion and conservation of heat reduce to Stokes flow with variable viscosity

$$u_x + v_y = 0, \tag{2.6}$$

$$p_x = 2\partial_x[\mu(T)u_x] + \partial_y[\mu(T)(u_y + v_x)], \tag{2.7}$$

$$p_y = 2\partial_y[\mu(T)v_y] + \partial_x[\mu(T)(u_y + v_x)], \tag{2.8}$$

and

$$T_t + uT_x + vT_y = T_{xx} + T_{yy}, \tag{2.9}$$

where here and in the rest of the paper we have dropped hats on dimensionless variables. The far-field boundary conditions are given by

$$T \to 1 \quad \text{and} \quad (u, v) \to (2x, -2y) \quad \text{as} \quad y \to \infty. \tag{2.10}$$

We assume the strained fluid has a much greater viscosity than its environment so that its surface can be taken to be stress free. The kinematic, zero-stress and radiation boundary conditions give

$$\eta_t + u\eta_x = v \quad \text{at} \quad y = \eta(x, t), \tag{2.11}$$

$$\boldsymbol{\Sigma} \cdot \boldsymbol{n} = 0 \quad \text{at} \quad y = \eta(x, t), \tag{2.12}$$

$$\mathscr{S}\boldsymbol{n} \cdot \nabla T = \left(T + \frac{T_c}{T_h - T_c}\right)^4 - \left(\frac{T_c}{T_h - T_c}\right)^4 \quad \text{at} \quad y = \eta(x, t), \tag{2.13}$$

where $\boldsymbol{\Sigma}$ is the stress tensor, $\boldsymbol{n}$ the normal to the free surface,

$$\mathscr{S} \equiv \frac{\rho c_p}{\sigma_B \alpha (T_h - T_c)^3}\left(\frac{\Gamma\kappa}{2}\right)^{1/2}, \tag{2.14}$$

α is the absorptivity and σ_B the Stefan–Boltzmann constant. We assume $T_h - T_c \gg T_c$ so that

$$\mathscr{S}\boldsymbol{n} \cdot \nabla T = T^4 \quad \text{at} \quad y = \eta(x, t). \tag{2.15}$$

The parameter $\mathscr{S}$ is a measure of the importance of the advection of heat by the straining flow relative to the radiative heat loss to the overlying environment. Small $\mathscr{S}$ corresponds to the case of a weak straining flow or of strong radiative cooling and thus the surface temperature will be close to the temperature of the overlying environment. Large $\mathscr{S}$ corresponds to the case of a strong straining flow or of weak radiative cooling and thus the surface temperature will be close to the temperature of the fluid at depth.

The relationship between viscosity and temperature will depend on the fluid in

question and must, in general, be determined empirically. For simplicity, we consider the one-parameter functional form

$$\mu(T) = \exp[\mathscr{B}(1 - T)], \tag{2.16}$$

which gives good experimental agreement, often over quite large temperature variations, for a wide range of fluids including lubricating oils, glycerol and most viscous syrups. The parameter $\mathscr{B}$ is a measure of the sensitivity of viscosity to temperature and an isoviscous fluid is represented by $\mathscr{B} = 0$. The value of $\mathscr{B}$ in lava flows can be estimated from graphs of the logarithm of viscosity versus temperature (e.g. Ryan & Blevins 1987) and the formula

$$\mathscr{B} = -\frac{\mathrm{d}\ln(\mu_{dim})}{\mathrm{d}T_{dim}}(T_h - T_c), \tag{2.17}$$

where the subscript *dim* refers to the dimensional quantities.

3. Steady solution

The steady-state solution is given by

$$(u_0, v_0) = (2x, -2y), \tag{3.1}$$

$$\eta_0 = 0, \tag{3.2}$$

$$T_0(y) = T_s + \frac{T_s^4}{\mathscr{S}}\int_0^y \mathrm{e}^{-z^2}\mathrm{d}z, \tag{3.3}$$

where T_s is the temperature at the surface, which satisfies the quartic equation (figure 2)

$$\frac{\pi^{1/2}}{2\mathscr{S}}T_s^4 + T_s - 1 = 0. \tag{3.4}$$

The deviatoric stress tensor corresponding to this flow is

$$\begin{bmatrix} 4\mu[T_0(y)] & 0 \\ 0 & -4\mu[T_0(y)] \end{bmatrix}. \tag{3.5}$$

Since $\boldsymbol{\Sigma}_{0yy} = 0$, we have $p_0(y) = -4\mu[T_0(y)]$ and

$$\boldsymbol{\Sigma}_0 = \begin{bmatrix} 8\mu[T_0(y)] & 0 \\ 0 & 0 \end{bmatrix}. \tag{3.6}$$

4. Stability

We now subject the steady solution to infinitesimal perturbations of the form

$$u = u_0 + u'(y)A(t)\mathrm{e}^{\mathrm{i}k(t)x}, \tag{4.1a}$$

$$v = v_0 + v'(y)A(t)\mathrm{e}^{\mathrm{i}k(t)x}, \tag{4.1b}$$

$$T = T_0 + T'(y)A(t)\mathrm{e}^{\mathrm{i}k(t)x} \tag{4.1c}$$

and

$$\eta = \eta' A(t)\mathrm{e}^{\mathrm{i}k(t)x}. \tag{4.1d}$$

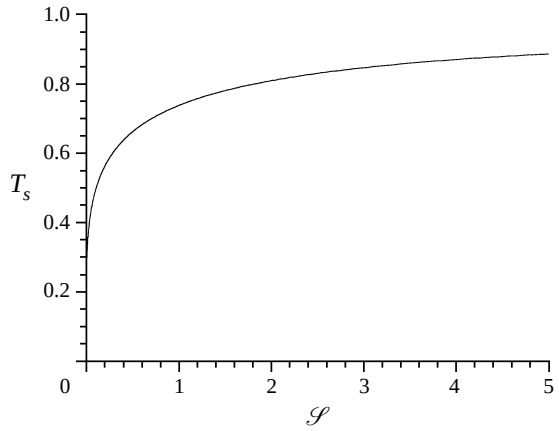

FIGURE 2. The basic-state surface temperature shows a rapid rise and slow asymptote with $\mathscr{S}$. The surface temperature is later used to define an effective viscosity contrast.

The wavenumber $k(t)$ is chosen to depend on time according to

$$k_t + 2k = 0 \tag{4.2}$$

in order to account for the horizontal stretching of modes by the steady-state straining flow (Tomotika 1936; Lister 1989). We define an instantaneous growth rate $\sigma(k)$ by

$$\sigma[k(t)] = \frac{A_t}{A}. \tag{4.3}$$

Substitution and linearization in the perturbation quantities followed by elimination of the pressure from the momentum equation yields

$$[\partial_y^2 + k^2][\mu(v'_{yy} + k^2 v')] = 4k^2 \partial_y[\mu v'_y - 2\mu_T T'], \tag{4.4}$$

where μ and $\mu_T \equiv \mathrm{d}\mu/\mathrm{d}T$ are both evaluated at $T = T_0(y)$.

The perturbation equation for the temperature is not fully separable. In order to proceed, we project onto modes of the form (4.1) by making a frozen-field approximation in which we neglect the time-variation of the wavenumber in the y-dependence of the modes. The resultant equation,

$$\sigma T' - 2y T'_y + v' T_{0y} = T'_{yy} - k^2 T', \tag{4.5}$$

shows the key effects of advection of temperature perturbations by the basic flow, advection of the basic temperature by the perturbed flow and diffusion. Hence, we do not expect the dynamical behaviour to be significantly affected by the projection.

The radiation boundary condition, kinematic boundary condition and zero-stress conditions at the free surface yield, respectively,

$$\mathscr{S}^2 T'_y = 4T_s^7 \eta' + 4\mathscr{S} T_s^3 T' \quad \text{at} \quad y = 0, \tag{4.6}$$

$$(\sigma + 2)\eta' = v' \quad \text{at} \quad y = 0, \tag{4.7}$$

$$v'_{yy} + k^2 v' = 8k^2 \eta' \quad \text{at} \quad y = 0, \tag{4.8}$$

$$v'_{yyy} - 3k^2 v'_y + 8k^2 \frac{\mu_T}{\mu}\left(\eta' T_{0y} + T'\right) \quad \text{at} \quad y = 0. \tag{4.9}$$

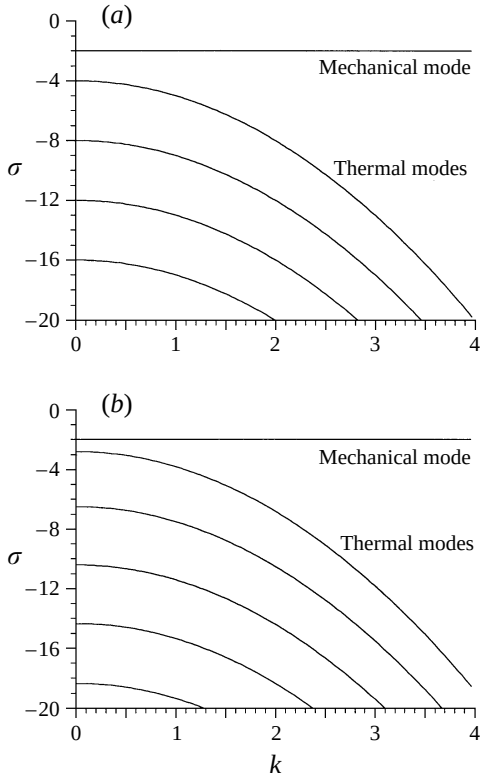

FIGURE 3. Dispersion relations of a constant viscosity fluid for (*a*) $\mathscr{S} = 0$ and (*b*) $\mathscr{S} = 1$. The thermal modes have quadratic variation (4.12) with wavenumber. The mechanical mode has $\sigma = -2$ corresponding to kinematic stretching by the basic flow.

The far-field boundary conditions are

$$v' \to 0 \quad \text{as} \quad y \to \infty, \tag{4.10}$$

$$T' = o(y^{(\sigma+k^2)/2}) \quad \text{as} \quad y \to \infty. \tag{4.11}$$

One of the linearly independent solutions of (4.5) is exponentially small at infinity, whereas the other has behaviour $T' \sim y^{(\sigma+k^2)/2}$. Therefore, (4.11) is equivalent to $T' \to 0$ when $\sigma + k^2 > 0$ and stronger than $T' \to 0$ when $\sigma + k^2 < 0$. The reason for the stronger condition is that slow algebraic decay of T' would cause the velocity field at infinity to be dominated by the response to the temperature perturbation at infinity, which we discount on physical grounds. In the context of this study, we are actually only interested in eigenmodes with $\sigma + k^2 > 0$, since other modes must be stable, and hence $T' \to 0$ would suffice.

The perturbation equations (4.4)–(4.11) form an eigenvalue problem for the growth rate σ. It is instructive to consider the simple case of constant viscosity (i.e. $\mu(T) \equiv 1$) for which it is found that there are two distinct types of modes (figure 3). First, there is a set of eigenmodes which we denote as *thermal modes* since they correspond to diffusive decay of temperature perturbations with a zero surface displacement and zero velocity perturbation. Solution of (4.5), (4.6) and (4.11) with $\eta = v' = 0$ shows that there is a countable infinity of such modes with the dependence of growth rate

on wavenumber given by

$$\sigma_j(k) = \sigma_j(0) - k^2, \quad \text{where} \quad j = 1, 2, \ldots . \tag{4.12}$$

For $\mathscr{S} = 0$ the eigenfunctions are given by the product of e^{-y^2} and Hermite polynomials, and $\sigma_j(0) = -4j$. Secondly, there is a single *mechanical mode* which arises from the fact that the steady-state straining flow stretches horizontal lengths and compresses vertical lengths. Thus any surface perturbation will be flattened by this process with a growth rate

$$\sigma = -2 \tag{4.13}$$

which is independent of wavenumber. This can be seen from the perturbation kinematic boundary condition. When $\sigma = -2$ we set $\eta' = 1$ (without loss of generality) and solve the resulting boundary-value problem to obtain the eigenfunctions.

5. Results

The numerical method employed to solve the eigenvalue problem was a shooting technique that takes into account the behaviour of the solutions at infinity (Appendix A). Starting from the above solutions for an isoviscous fluid, we slowly increased the viscosity contrast and tracked the eigenmodes using a continuation scheme.

For sufficiently large viscosity variations the behaviour at very small wavenumber is quite complex (Appendix B). This behaviour appears never to affect the stability of the flow and thus is not of great interest here. However, the small-wavenumber asymptotics can be derived and provide a useful check on the numerical method.

Extensive tests showed that the mechanical mode always becomes unstable prior to any of the thermal modes and hence from now on we concentrate on the mechanical mode.

For weak radiative cooling (rapid straining, $\mathscr{S} \gg 1$) the surface temperature is close to the temperature at depth and therefore the actual contrast in viscosity within the fluid is much smaller than the contrast in viscosity that might exist between the fluid at depth and fluid at the temperature of the overlying environment. For this reason, we introduce the effective viscosity contrast

$$\mu_s \equiv \frac{\mu(T_s)}{\mu(1)} = \mu(T_s), \tag{5.1}$$

which represents the ratio of unperturbed surface viscosity to the viscosity at depth. The basic-state viscosity profile takes the form

$$\mu(T_0(y)) = \mu_s^{[1-\mathrm{erf}(y)]}, \tag{5.2}$$

which is independent of $\mathscr{S}$ at fixed μ_s, though it depends on $\mathscr{S}$ at fixed $\mathscr{B}$. The form of (5.2) suggests that μ_s is a useful measure of the viscosity contrast within the fluid.

The results for $\mathscr{S} = 0$ are shown in figure 4(*a*). This corresponds to the case of infinitely strong radiative cooling (or infinitely weak straining) in which the surface temperature is constrained to be zero. As the viscosity contrast μ_s increases from small to moderate values, the mechanical mode becomes considerably more stable than the isoviscous case. As μ_s becomes very large, the stabilizing effect decreases, but the mode remains more stable than the isoviscous case. For all $\mu_s > 1$ the mechanical mode is very stable for large wavenumbers because of the strong thermal diffusion on these short lengthscales.

For weaker radiative cooling ($\mathscr{S} > 0$) the results for small viscosity contrast μ_s

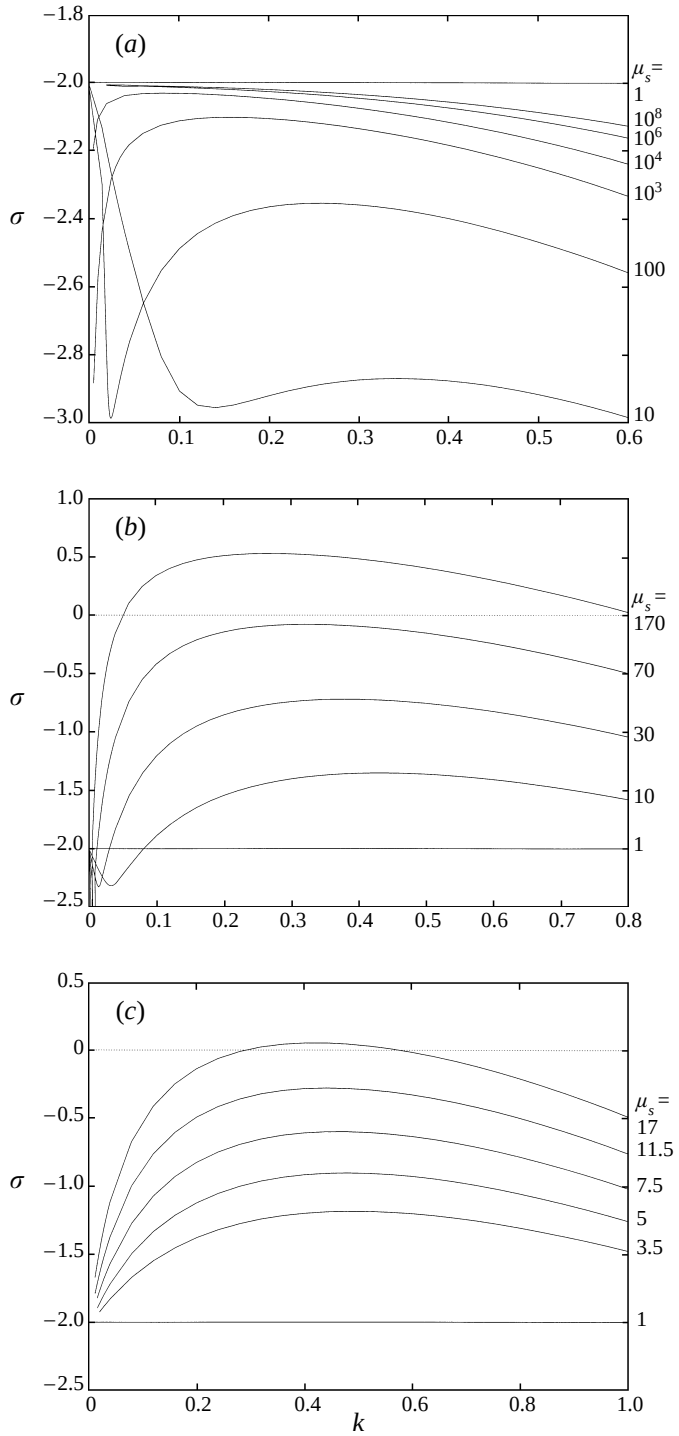

FIGURE 4. Dispersion relation of the mechanical mode at various values of the effective viscosity contrast μ_s. (*a*) $\mathscr{S} = 0$. Stabilization for $\mu_s < 10$ is reduced at large μ_s, but not sufficiently to cause instability. (*b*) $\mathscr{S} = 1$. For sufficiently large μ_s instability occurs over a finite band of wavenumbers. (*c*) $\mathscr{S} = 100$.

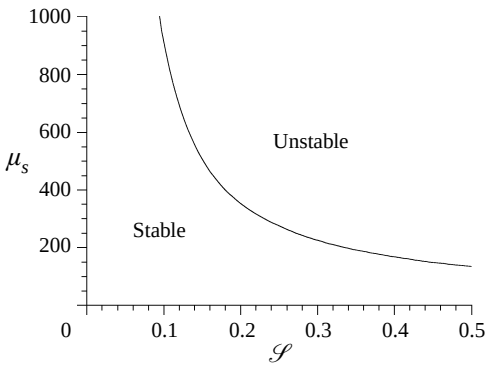

FIGURE 5. The critical effective viscosity contrast μ_s for which instability occurs as a function of $\mathscr{S}$.

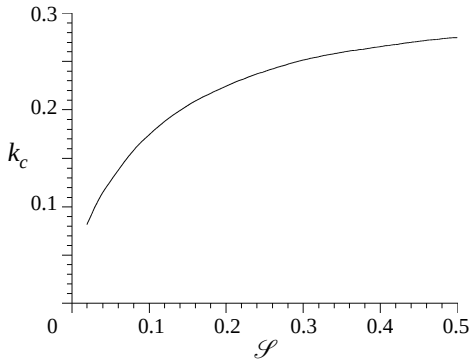

FIGURE 6. The critical wavenumber at which instability occurs as a function of $\mathscr{S}$.

are qualitatively similar to the results for $\mathscr{S} = 0$ with the mechanical mode initially becoming more stable at all wavenumbers as μ_s increases. However, the results for moderate to large viscosity variations are significantly different. At small and large wavenumbers for $\mathscr{S} = 1$ (figure 4*b*) the mechanical mode remains more stable than the isoviscous case. However, intermediate wavenumbers are made less stable by increasing viscosity contrast. At a critical value of the viscosity contrast there is a neutral mode for a single critical wavenumber and if the viscosity contrast is larger than this critical value there is a finite band of unstable wavenumbers. For even weaker radiative cooling ($\mathscr{S} = 100$, figure 4*c*) the behaviour is similar with instability occurring at lower effective viscosity contrasts.

In figures 5 and 6 the critical effective viscosity contrast and the critical wavenumber for which instability occurs are plotted as functions of $\mathscr{S}$. The required effective viscosity contrast μ_s decreases monotonically with $\mathscr{S}$. In figure 7 the critical total viscosity contrast $\mathscr{B}$ is plotted against $\mathscr{S}$. As might be anticipated from figure 5, for small values of $\mathscr{S}$ the critical viscosity contrast decreases with increasing $\mathscr{S}$. However, for large $\mathscr{S}$ the surface temperature very rapidly approaches the temperature of the fluid at depth (figure 2) and so extremely large values of $\mathscr{B}$ are needed to achieve the required effective viscosity contrasts.

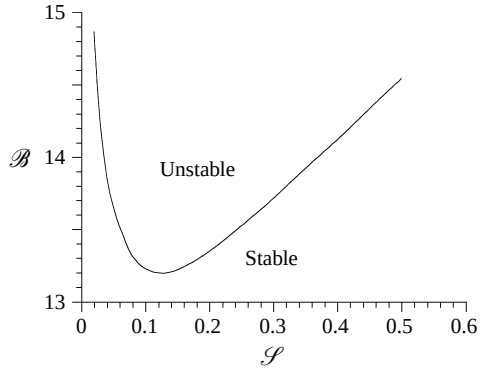

FIGURE 7. The critical total viscosity contrast (2.17) for which instability occurs as a function of $\mathscr{S}$. This contrast based on the cold ambient temperature is much greater than the effective contrast based on the warmer surface temperature (see figures 2 and 5).

6. Discussion and physical mechanism

We have used a modified linear stability analysis to determine the conditions under which the cooled surface of a fluid with temperature-dependent viscosity becomes unstable under the influence of a straining flow. Both high and low wavenumbers are found to be stable. Instantaneous growth occurs for sufficiently small $\mathscr{S}$ and large $\mathscr{B}$ in a finite band of wavenumbers. Since the wavelength of any disturbance is continuously stretched by the steady-state straining flow, we must consider the time dependence of the growth and decay of any given disturbance. A disturbance which begins at short wavelength (high wavenumber) will initially decay. As the wavelength of the disturbance is stretched by the straining flow, the wavenumber decreases and growth of the disturbance will occur while in the finite band of wavenumbers. If the amplitude of the disturbance remains sufficiently small that the linear theory is valid during this period of growth then the wavenumber eventually decreases sufficiently that the disturbance once again decays. However, if the amplitude of the disturbance becomes sufficiently large that nonlinear effects become important then surface disturbances may experience sustained nonlinear growth.

The mechanism driving the instability can be understood in the following terms. Suppose we make a small temperature increase in a region in the interior of the fluid so that the local viscosity decreases there. This region of less viscous fluid cannot support the imposed basic-state horizontal stress field and therefore will stretch horizontally faster than in the basic state. As the fluid element is stretched it must, by continuity, induce a vertical flow. The fluid above the fluid element is cold and therefore more viscous than the hot fluid below and so the stretching will preferentially draw in the hot fluid from below. This upward advection of heat can cause a further increase in temperature in the region. This provides a feedback mechanism which acts to destabilize the flow.

The variation of critical effective viscosity contrast μ_s with $\mathscr{S}$ can be understood as follows. For strong radiation (weak straining, $\mathscr{S} \ll 1$), any temperature perturbation at the surface is strongly constrained to be close to zero, whereas for weak radiation (strong straining, $\mathscr{S} \gg 1$), the surface temperature is easily affected by local variations in the strain rate. This affects the stability in two ways. First, since basic-state viscosity contrasts are greatest near the surface, the feedback mechanism described above is most effective when the temperature perturbation at the surface can be large.

Secondly, when the temperature perturbation at the surface is weakly constrained the eigenmodes have smaller gradients in temperature near the surface and so are less strongly stabilized by thermal diffusion. Both of these effects mean that instability occurs more readily for weak radiation (strong straining, $\mathscr{S} \gg 1$).

A counteracting effect is that for very weak radiative cooling (strong straining $\mathscr{S} \gg 1$) the steady-state temperature profile is close to isothermal, with only very weak gradients. Consequently, the vertical flow induced by the stretching of a fluid element can only advect very small amounts of heat. Hence the above feedback mechanism becomes less effective. However, this effect is small when compared with the two effects relating to the surface temperature discussed above. Thus, at large $\mathscr{S}$ instability occurs more readily (figure 5). This is rather surprising, in that one might naively imagine that the instability would occur most vigorously for strong cooling.

In the context of the formation of surface features in lava flows the total viscosity variation $\mathscr{B}$ is fixed. When the hot lava from the interior breaks through a weak point in the surface rapid inflation of the lava front occurs initially so that the initial strain rates, and therefore $\mathscr{S}$, are large. Thus the surface temperature is close to the temperature of the hot lava from the interior and so the effective viscosity variation between the lava at depth and the lava at the surface is small and therefore the flow remains stable (figure 7). As the breakout of lava increases in size, the strain rate and, therefore, $\mathscr{S}$, decrease. If $\mathscr{B}$ is sufficiently small then instability will never be realized. However, if $\mathscr{B}$ is sufficiently large, when $\mathscr{S}$ decreases into the unstable region (figure 7) surface features on a lengthscale of $(\kappa/\Gamma)^{1/2} \sim 1$ mm–1 cm are formed. When $\mathscr{S}$ subsequently decreases below the critical value for instability of a smooth surface the surface features may either decay, experience nonlinear growth or, if the flow is cooling very rapidly, be frozen in. These processes dictate the observed morphology of the advancing lava front.

In conclusion, our analysis has identified a new instability induced by surface cooling of a viscous fluid undergoing extension. We have considered the simplest and most fundamental problem but we believe that the instability mechanism will apply to more complicated flows and thus have a wide variety of applications. For example, suppressing surface instabilities in industrial processes such as glass manufacture is of obvious importance. Despite the complexity of lava flows, this work also makes a step towards understanding the mechanisms which give rise to their surface morphology.

Appendix A. Numerical method

The main issue to be addressed by the numerical shooting scheme is implementation of the boundary conditions (4.10) and (4.11). At infinity the temperature perturbation takes the form

$$T' \sim A_1\mathscr{F}_1(y) + A_2\mathscr{F}_2(y) + \text{ exponentially small coupling terms}, \tag{A 1}$$

where $\mathscr{F}_1(y) \sim y^{(\sigma+k^2)/2}$ and $\mathscr{F}_2(y)$ as $y \to \infty$. The velocity perturbation takes the form

$$v' \sim (A_3 y + A_4)\mathrm{e}^{ky} + A_1\mathscr{R}_1(y) + (A_5 y + A_6)\mathrm{e}^{-ky} + \text{ exponentially small coupling terms}, \tag{A 2}$$

where $\mathscr{R}_1 \sim by^{(\sigma+k^2-2)/2}$ is the response to $\mathscr{F}_1$ in the momentum equation; $A_1, \ldots, A_6$ and b are constants and (4.10) and (4.11) require $A_1 = A_3 = A_4 = 0$.

For fixed k and σ, solution of (4.4)–(4.9) gives a linear relationship between initial values $v'(0)$, $v'_y(0)$ and $T'(0)$ and the far-field constants A_1, A_3 and A_4. We integrate

three linearly independent sets of initial conditions to $y = M$ using a fourth-order Runge–Kutta method, where M is chosen such that the exponentially small terms have a magnitude less than the computational round-off error. In practice $M = 5$ is sufficient. The corresponding values of A_1 are extracted from (A 1) and the relationship between $v'(0)$, $v'_y(0)$ and $T'(0)$ that makes $A_1 = 0$ is determined. Within this subspace of initial conditions, the term $\mathscr{R}_1(y)$ in (A 2) is not present and the values of A_3 and A_4 are then easily obtained from the values of v' and its derivatives at $y = M$. We can thus construct a matrix $\mathscr{L} \equiv \mathscr{L}(\sigma, k)$ such that

$$\begin{pmatrix} A_3 \\ A_4 \end{pmatrix} = \mathscr{L} \begin{pmatrix} v'(0) \\ v'_y(0) \end{pmatrix}, \tag{A 3}$$

and find eigensolutions with $A_3 = A_4 = 0$ by solving for $\sigma(k)$ from the roots of $\det[\mathscr{L}(\sigma, k)] = 0$.

Appendix B. Small-wavenumber behaviour

When the viscosity is not constant the mechanical mode still has growth rate $\sigma = -2$ at $k = 0$ since large-wavelength perturbations are insensitive to the viscous surface layer. Asymptotic analysis of the limit $k \to 0$ is rather lengthy, requiring matching between expansions for $y = O(1)$ and $y = O(k^{-1})$ to be taken to fourth order before an $O(k)$ correction to $\sigma = -2$ can be calculated (Wylie 1997). Numerically it is found that for very small values of the wavenumber ($k \ll 1$) the growth rate of the mode decreases linearly and rapidly as the wavenumber increases. At a still smaller value of k the growth rate of the mechanical mode collides with the growth rate of the first thermal mode and both growth rates become complex. However, with a further increase in k the modes recollide and become real again. The growth rate of the mechanical mode remains real for further increases in wavenumber.

REFERENCES

Crisp, J. & Baloga, S. 1990 A model for lava flows with two thermal components. *J. Geophys. Res.* **95**, 1255.

Fink, J. H. & Griffiths R. W. 1990 Radial spreading of viscous-gravity currents with solidifying crust. *J. Fluid Mech.* **221**, 485.

Hulme, G. 1974 The interpretation of lava flow morphology. *Geophys. J. R. Astron. Soc.* **39**, 361.

Huppert, H. E. 1982 The propagation of two-dimensional and axisymmetric viscous gravity currents over a rigid horizontal surface. *J. Fluid Mech.* **121**, 43.

Keszthelyi, L. & Denlinger, R. 1996 The initial cooling of pahoehoe flow lobes. *Bull. Volcanol.* **58**, 5.

Lister, J. R. 1989 Selective withdrawal from a viscous two-layer system. *J. Fluid Mech.* **198**, 231.

Lister, J. R. 1992 Viscous flows down an inclined plane from point and line sources. *J. Fluid Mech.* **242**, 631.

Ryan, M. P. & Blevins J. Y. K. 1987 The viscosity of synthetic and natural silicate melts and glasses at high temperatures and 1 bar pressure and at high pressures. *US Geol. Surv. Surv. Bull.* **1764**, 1.

Stasiuk, M. V., Jaupart, C. & Sparks, R. S. J. 1993 Influence of cooling on lava-flow dynamics. *Geology* **21**, 335.

Tepley, L. & Moore, J. G. 1974 Fire under the sea: the origin of pillow lava. 16 mm Sound Motion Picture, Moonlight Productions, Mountain View, California, USA.

Tomotika, S. 1936 Breaking up of a drop of viscous fluid immersed in another viscous liquid which is extending at a uniform rate. *Proc. Roy. Soc. Lond.* A **153**, 302.

Wylie, J. J. 1997 Geological fluid mechanics. PhD thesis, University of Cambridge.